Results from the Luminosity Oscillations Imager on board SOHO: low-degree p-mode parameters for a 2-year data set.

T.Appourchaux[1] and the VIRGO team

[1] Space Science Department of ESA, ESTEC, NL-2200 AG Noordwijk, (thierrya@so.estec.esa.nl)

ABSTRACT

I report on the results from a 2-year LOI time series starting on March 27, 1996 and ending on March 26, 1998. From the data set, I have analysed independently two 1-year time series mainly for minimizing the effect of solar activity. For $l \leq 5$ the p-mode data are fitted using the Fourier spectra taking into account the mode leakage and noise correlations. For $l \geq 6$, the small number of pixels (12) lead to undersampling that result into non-invertible leakage matrices: the Fourier spectra cannot be utilised anymore. In addition for these degrees, the spectra of the l=4,5,6 modes are strongly polluted by the l=7,8, 1 modes, and vice versa. Due to these two major problems, I have fitted simultaneously the power spectra of l=4,7, l=5,8 and l=1,6; this is clearly an approximation that will lead to systematic errors.

I give tables of frequencies, splittings and linewidths for the 2-year data set. The splittings are compared with other data sets such as LOWL, MDI and GONG. The effects of the solar activity is also studied.

Key words: intensity - p modes - SOHO - Sun

1. Introduction

The Luminosity Oscillations Imager (LOI) is a small instrument part of the VIRGO instrument aboard SOHO. The instrument was described by Appourchaux et al (1995) and its in-flight performances were given by Appourchaux et al (1997). One of the scientific goals of the LOI is to detect low-degree solar p modes in intensity. In this paper I report on the first useful scientific results of the LOI. In the first 2 sections, I explain how the data are reduced for extracting from the pixel intensity the useful spectra. In the third section, I show how the spectra are fitted for obtaining the p-mode parameters. In the last sections, I show the results obtained and address the source of systematic errors and then conclude.

2. Data reduction

The LOI time series analysed here starts on 27 March 1996 0:00 TAI and ends on 26 March 1998 23:59 TAI. The level-0 data are acquired from the VIRGO data center in Tenerife (Jiménez et al., 1998). The data are then calibrated to engineering units and corrected from temperature effects and pixel sensitivity variations. Since the spacecraft orbit around the L1 point of the Sun-Earth system, the apparent size of the solar image varies along the orbit. A first order correction of this variation is applied for obtaining the pixel intensity as it would have been observed at 1 AU. In addition a relativistic correction is applied taking into account the spacecraft velocity; this is a minute correction. All these corrections are described in the LOI VDC document available on the VIRGO home page under virgo.so.estec.esa.nl/html/software.html. After all these corrections the level-1 data are ready to be used. For studying the effect of activity, I have extracted two 1-year time series from the initial 2-year data set.

3. Mode extraction

The 12 pixel time series are then detrended using a 2-day triangular filter. Using this detrending, the relative variation for each pixel are derived. Spikes larger than 5 σ are replaced by zeros. Missing data are also replaced by zeros. The data can now be combined to extract the signals.

For combining the data, Appourchaux and Andersen (1990) described a filtering scheme called *optimal filtering*. This scheme was used both by Appourchaux et al.(1995) and by Rabello-Soares et al.(1997). Since then the filtering technique have evolved towards simplicity. The optimal filtering can be done later after having combined the data with *natural* filters, i.e. using spherical harmonics decomposition. Examples of *a posteriori* optimal filtering can be found in Appourchaux et al.(1998b) and in the invited review on low-degree splittings by the same author.

The spherical harmonics decomposition is computed as in Appourchaux and Andersen (1990) using the limb darkening derived from Allen (1973). The filters are normalized according to Eqs (17) of Appourchaux et al.(1998a). This normalization allows to have a symmetrical leakage matrix (Appourchaux et al., 1998a). Example of such leakage matrix can be found in Appourchaux et al.(1998b). Since the apparent solar diameter changes along the orbit, the spherical harmonic filters vary slowly with time. To alleviate this problem, time-independent filters are applied to the pixels for extracting the (l, m) modes. The filters are computed as an average over 1 year of filters computed weekly. Over this period the B angle has a mean close to zero. Gizon et al.(1997) showed that it was possible to detect the influence of a non-zero B angle on the p-mode data. Therefore, this average minimizes the effect of the B angle on the data. After combining the pixels with the filters, the time series are Fourier transformed; the positive frequencies provide the signal for $+m$, and the negative frequencies provide the conjugate of the signal for $-m$ (Appourchaux et al., 1998a).

4. Spectra fitting

The fitting of the data is done using 2 different techniques:

- Maximum Likelihood estimation of Fourier spectra for $l \leq 5$
- Maximum Likelihood estimation of power spectra for $l \geq 4$

Each technique is described hereafter in more detail.

4.1 Fourier spectra fitting

This technique was introduced by Schou (1992) and later refined by Appourchaux et al.(1998a). The method relies on the knowledge of the leakage matrix for inferring the p-mode parameters. This method can only be applied when the leakage matrix can be inverted (Appourchaux et al., 1998a). For the LOI, the leakage matrix cannot be inverted for $l \geq 6$. This is because the number of pixels (N) will allow to resolve only modes with $l \leq [(N-1)/2]$, i.e. for the LOI, $l_{max} = 5$. Therefore, I applied this technique for $l \leq 5$.

When fitting power spectra, it is usually convenient to visualize an estimate of the variance of the power spectra. For instance, one can visualize a smoothed power spectra which is a good estimate of the variance. In our case, it is also convenient to visualize smoothed cross spectra of the different l, m signals or even better echelle diagrams of these spectra (Appourchaux et al., 1998b). Figure 1 shows a *covariance diagram* for $l = 2$ that gives estimate of the covariance of the cross spectra (On the CD-ROM supplement, see file `mmm/appour_2/figure1.ps`).

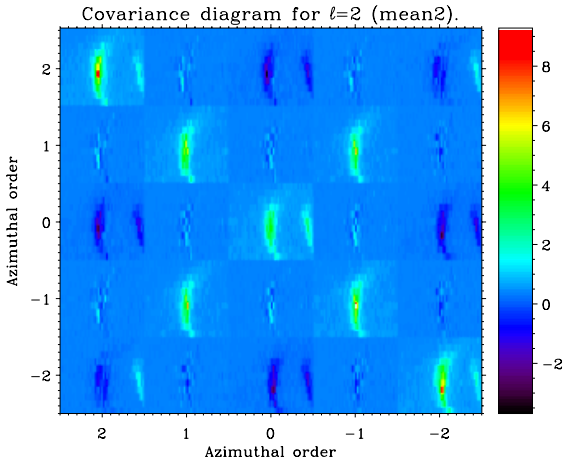

Figure 1: Covariance diagram of $l = 2$ for the LOI data. This diagram is made of 25 echelle diagrams of the real parts of the cross spectra of m and m'. The diagonal represents the usual power spectra. Correlations between the $2l + 1$ signals can be clearly seen especially when $m + m'$ is even. The $l = 0$ ridge can be seen at the right-hand side of the $l = 2$ ridge.

4.2 Power spectra fitting

Unfortunately, there is an additional problem that need also to be solved: the presence of aliasing modes. For example, the $l = 1$ modes are polluted by $l = 6$ and $l = 9$ modes the $l = 4$ modes by the $l = 7$ modes, the $l = 5$ modes by the $l = 8$ modes, and vice versa. If the leakage matrix can be inverted, it is possible to fit simultaneously the target and aliasing modes (Appourchaux et al., 1998a). Instead, it is somewhat easier to apply the inverse of the leakage matrix to clean the data of the target modes from the aliasing modes, and vice versa (Appourchaux et al., 1998a). This procedure has been successfully applied to the GONG data (Rabello-Soares and Appourchaux, these proceedings). Unfortunately the leakage matrices for $l > 5$ cannot be inverted and the LOI data cannot be cleaned. An alternative fitting was devised in which both power spectra of the target mode and of the aliasing mode were simultaneously fitted. Figure 2 shows the variance of the spectra that were actually fitted for $l = 4$ and $l = 7$ (On the CD-ROM supplement, see files `mmm/appour_2/figure2a.ps` and `mmm/appour_2/figure2b.ps`). In this case we neglected all correlations between the target (l, m) signal and the other (l', m') signals. I used the power spectra of both degrees mainly for reducing systematics effects on the frequency determination. This approximation is likely to introduce systematic errors in the determination of other parameters such as the splitting and the linewidth. This is the reason why I also used the Fourier spectra fitting technique in order to study systematic effects for $l = 4$ and $l = 5$.

5. Results

I have fitted the data using the techniques described above. The model of the p-mode profile was assumed to be a lorentzian. The splittings were decomposed using Clebsh-Gordan coefficients as in Ritzwoller and Lavelly (1991). Three pixel noises were used for modeling the solar noise (Appourchaux et al., 1998a). The leakage and noise covariance matrix were derived from Appourchaux et al., 1998a. I did not include asymmetry in the profile nor a slope in the noise.

5.1 Systematic errors

I have also studied the effect of fitting the $l = 4$ and $l = 5$ with 2 different fitting techniques. Figure 3 shows the difference between the 2 techniques for the frequency, the linewidth and the splitting (On the CD-ROM supplement, see files `mmm/appour_2/system_0.ps`, `mmm/appour_2/system_1.ps`,`mmm/appour_2/system_2.ps`. The impact on frequency determination is huge. The linewidth with the power spectra are so much overestimated that the dip observed in the VIRGO data by Fröhlich et al.(1997) cannot be detected anymore. The splittings are also strongly affected. The source of the systematic errors related to the fitting techniques is well understood:

- *Simultaneous power spectra fitting*: neglecting noise correlations between the (l, m) signals forces the minimization code to create larger linewidths and thereby smaller splittings.
- *Single degree Fourier spectra fitting*: neglecting the presence of aliasing modes into the target modes force the minimization code to shift the mode frequency toward the aliasing modes.

This is the main reason why I do not give table of linewidths and splittings for $l > 3$. I believe that the bias on the frequencies derived from fitting power spectra is minute and will only affect the error bars.

A new fitting scheme has to be devised for $l \geq 4$ that will allow to get unbiased estimated of all parameters at the same time. For example, one could fit simultaneously the power spectra but using a fixed linewidth depending on frequency. Since the linewidth is independent of the degree, an estimate of the linewidth could be derived from the $l \leq 3$ modes. The impact on the error bars of the other parameter has to be studied carefully. Another solution would be to decompose the signals into pseudo-signals for which the leakage matrix could be inverted.

The effect of asymmetry on the frequency determination has not been taken into account. It is well demonstrated that the low-degree p-mode frequencies depends upon

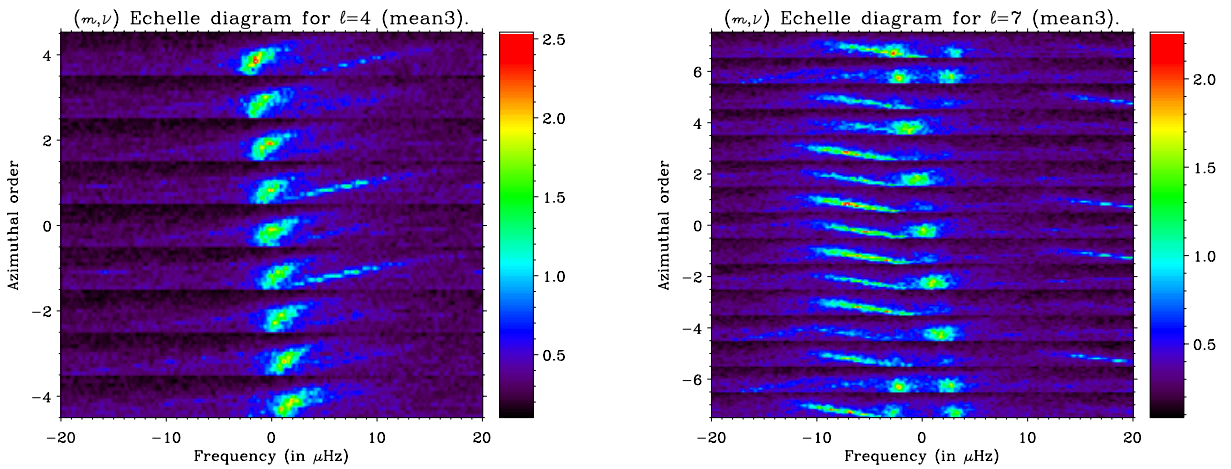

Figure 2: (m, ν) echelle diagrams: left, for $l = 4$; right, for $l = 7$. On the left diagram, the $l = 7$ modes appear as oblique ridges crossing from bottom left to top right. On the right diagram, the $l = 4$ modes cross from bottom right to top left.

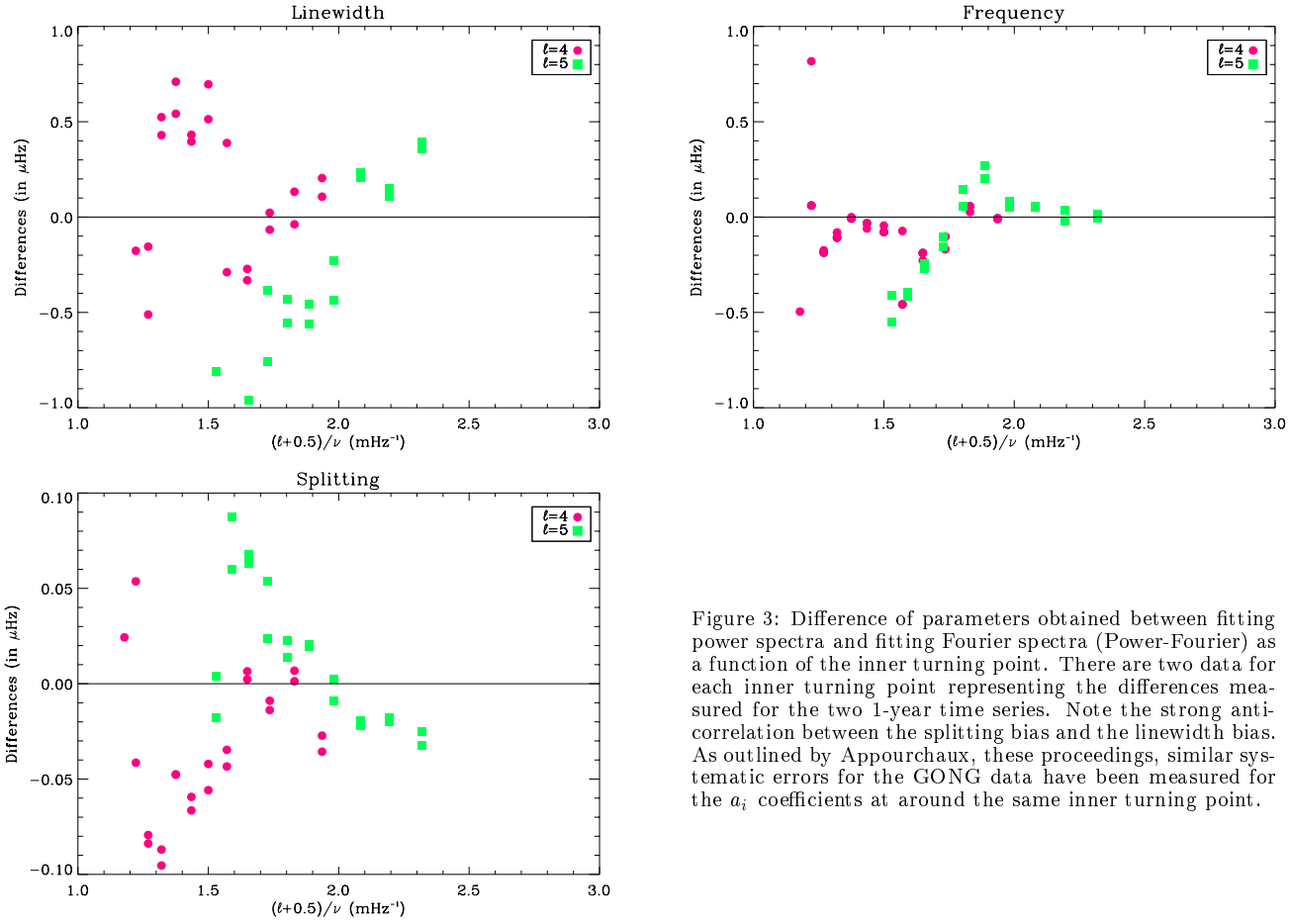

Figure 3: Difference of parameters obtained between fitting power spectra and fitting Fourier spectra (Power-Fourier) as a function of the inner turning point. There are two data for each inner turning point representing the differences measured for the two 1-year time series. Note the strong anti-correlation between the splitting bias and the linewidth bias. As outlined by Appourchaux, these proceedings, similar systematic errors for the GONG data have been measured for the a_i coefficients at around the same inner turning point.

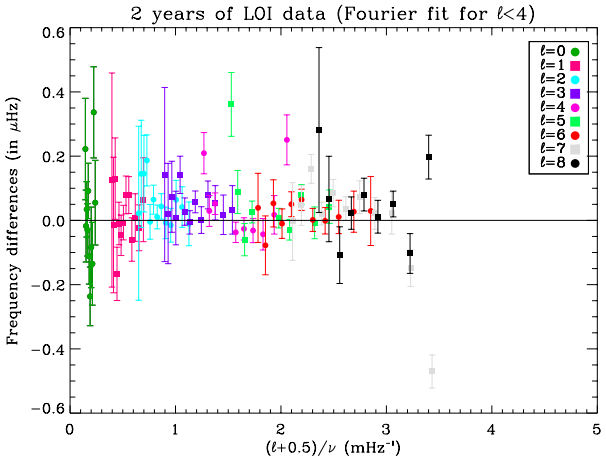

Figure 4: Frequency difference between the two 1-year data sets as a function of the inner turning point.

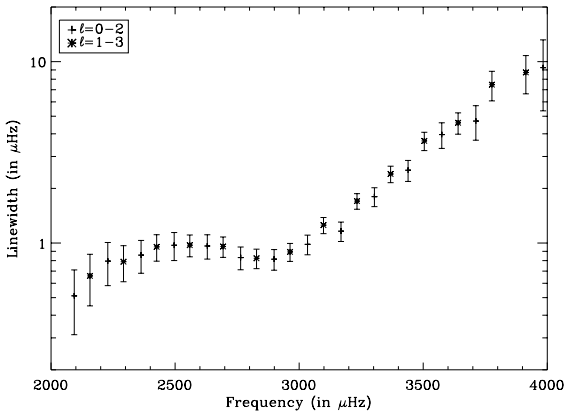

Figure 5: Linewidth as a function of frequency for pair of modes (l=0-2 and l=1-3). The error bars are 3-σ values. The dip at 2800 μHz is about 0.2 μHz.

which perturbation is observed, e.g. intensity or velocity (Toutain et al., 1997; Appourchaux et al., 1997). The source of the asymmetry of the line profile is related to correlation between the background noise and the modes (Nigam, these proceedings). In the near future, I will also take into account asymmetry into the solar p-mode line profile.

5.2 Effect of activity

Figure 4 shows the frequency difference between the 2 times series as a function of the inner turning point (On the CD-ROM supplement, see files `mmm/appour_2/figure4.ps`). A positive offset can clearly be seen which average over frequency and degree is about 25 $\pm$ 6 nHz. After Elsworth et al.(1994), the predicted frequency shift should be about 60 $\pm$ 7 nHz using the Wolf number, and 50 $\pm$ 7 nHz using the 10-cm Radio Flux (Solar indices taken from www.ngdc.noaa.gov/stp/SOLAR/getdata.html). These numbers are not inconsistent with each other meaning that the frequencies should be corrected from solar activity effects. Table 1 shows the frequencies for the 2-year data set. The two 1-year data set were merged after having applied a correction to each 1-year data set dependent upon frequencies and solar activity (Elsworth et al., 1994).

5.3 Linewidths

In Table 3, I give linewidths of the modes for which the systematics errors are small. As it is shown in a previous section the linewidths measured for $l > 3$ have large systematic errors due to the power spectra fitting technique. From Figure 5 the smaller linewidths at about 2800 μHz is an effect of resonance between convection and the oscillations affecting it (Gough, 1977). This small depression might only be detected with imaging instruments as full-disk integrated instruments could slightly overestimate the linewidth in this frequency range (Chaplin et al., 1997; Fierry-Fraillon et al., 1998). The dip was already detected in the VIRGO data by Fröhlich et al.(1997) but it was larger: about 0.4 μHz at 3000 μHz, to be compared to 0.2 μHz at about 2850 μHz in this paper. It

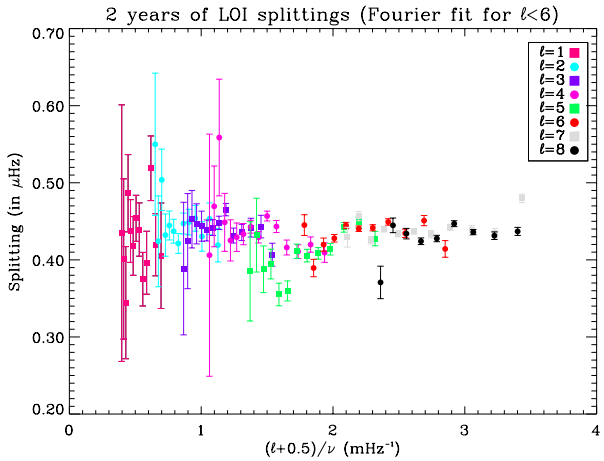

Figure 6: LOI sidereal splitting as a function of the inner turning point.

is also seen with the same characteristics in the GONG data by Rabello-Soares and Appourchaux, these proceedings. Theoretically, the size and the location of the dip depends upon the parameters modeling the convection (Houdek, 1996). If the dip does indeed vary with the solar activity, this would have very important implications for the interaction between convection, magnetic activity and the solar p modes; of course not to mention the impact on frequency measurements.

5.4 Splittings

Figure 6 shows the sidereal splittings as a function of the inner turning point (On the CD-ROM supplement, see file `mmm/appour_2/figure6.ps`). The splittings shown here are derived from Fourier spectra fitting for $l \leq 5$, and from power spectra fitting for $l \geq 6$. The systematic errors for the splitting are discussed in a previous section. There is no doubt that the splittings for $l > 3$ have large systematic errors. Nevertheless the splittings for $l \leq 3$ are likely to have very small systematic errors

Table 1: p-mode frequencies and their 1-σ error bars for the 2-year data set. The frequencies are corrected for 65. s.f.u (10-cm solar flux unit). The frequencies are derived from Fourier spectra fitting for $l \leq 3$, and from power spectra fitting for $l \geq 4$.

n	l=0	l=1	l=2	l=3
14	2093.546 ± 0.065	2156.925 ± 0.062	2217.786 ± 0.033	2273.511 ± 0.037
15	2228.717 ± 0.070	2292.024 ± 0.035	2352.297 ± 0.031	2407.746 ± 0.030
16	2362.878 ± 0.063	2425.671 ± 0.036	2485.962 ± 0.030	2541.710 ± 0.026
17	2496.266 ± 0.061	2559.249 ± 0.033	2619.666 ± 0.026	2676.223 ± 0.021
18	2629.765 ± 0.045	2693.387 ± 0.028	2754.509 ± 0.024	2811.453 ± 0.020
19	2764.135 ± 0.042	2828.143 ± 0.029	2889.578 ± 0.019	2947.040 ± 0.016
20	2899.010 ± 0.043	2963.218 ± 0.026	3024.715 ± 0.018	3082.255 ± 0.018
21	3033.752 ± 0.040	3098.033 ± 0.031	3159.868 ± 0.022	3217.703 ± 0.021
22	3168.617 ± 0.043	3233.138 ± 0.033	3295.055 ± 0.027	3353.501 ± 0.029
23	3303.312 ± 0.055	3368.572 ± 0.041	3430.821 ± 0.039	3489.679 ± 0.041
24	3438.934 ± 0.077	3504.303 ± 0.063	3566.820 ± 0.059	3626.256 ± 0.055
25	3574.797 ± 0.121	3640.539 ± 0.104	3703.476 ± 0.082	3763.026 ± 0.078
26	3712.136 ± 0.224	3776.920 ± 0.166	3840.547 ± 0.134	3900.338 ± 0.131
27	-	3913.726 ± 0.259	3977.387 ± 0.201	4037.968 ± 0.188

n	l=4	l=5	l=6	l=7	l=8
12	-	-	-	2184.193 ± 0.017	-
13	2188.520 ± 0.037	2235.445 ± 0.025	2279.941 ± 0.052	2322.346 ± 0.021	2362.910 ± 0.033
14	2324.232 ± 0.028	2371.253 ± 0.024	2415.539 ± 0.031	2458.244 ± 0.031	2499.569 ± 0.030
15	2458.637 ± 0.023	2506.144 ± 0.015	2551.113 ± 0.026	2594.289 ± 0.024	2636.113 ± 0.029
16	2592.973 ± 0.018	2641.242 ± 0.015	2687.049 ± 0.020	2731.156 ± 0.025	2773.818 ± 0.020
17	2728.466 ± 0.017	2777.303 ± 0.015	2823.731 ± 0.017	2868.361 ± 0.018	2911.628 ± 0.025
18	2864.184 ± 0.015	2913.656 ± 0.013	2960.617 ± 0.016	3005.617 ± 0.021	3049.148 ± 0.025
19	3000.094 ± 0.014	3049.858 ± 0.013	3097.175 ± 0.019	3142.752 ± 0.017	3186.613 ± 0.025
20	3135.885 ± 0.014	3186.236 ± 0.017	3233.809 ± 0.022	3279.790 ± 0.022	3324.189 ± 0.043
21	3271.713 ± 0.016	3322.725 ± 0.024	3370.484 ± 0.036	3417.342 ± 0.030	3462.294 ± 0.065
22	3408.114 ± 0.023	3459.526 ± 0.033	3508.072 ± 0.045	3554.913 ± 0.060	3600.642 ± 0.127
23	3544.771 ± 0.031	3596.805 ± 0.049	3646.106 ± 0.053	3695.956 ± 0.002	-

Table 2: LOI sidereal splittings (a_1 in nHz) and their 1-σ error bars for the 2-year data set.

n	l=1	l=2	l=3
14	405 ± 68	419 ± 22	407 ± 15
15	420 ± 40	453 ± 21	443 ± 15
16	519 ± 42	430 ± 19	442 ± 12
17	396 ± 41	454 ± 17	436 ± 11
18	375 ± 35	449 ± 17	432 ± 10
19	439 ± 35	447 ± 14	465 ± 8
20	454 ± 30	421 ± 13	448 ± 9
21	418 ± 38	437 ± 16	442 ± 10
22	437 ± 41	445 ± 19	438 ± 14
23	486 ± 50	432 ± 27	444 ± 19
24	345 ± 73	504 ± 40	447 ± 26
25	401 ± 104	424 ± 59	453 ± 37
26	435 ± 166	550 ± 92	424 ± 62
27	712 ± 245	642 ± 142	389 ± 86

Table 3: Linewidths (in μHz) and their 1-σ error bars for the 2-year data set.

n	l=0	l=1	l=2	l=3
14	0.342 ± 0.102	0.720 ± 0.141	0.632 ± 0.087	0.639 ± 0.079
15	0.702 ± 0.154	0.605 ± 0.098	0.818 ± 0.079	0.893 ± 0.074
16	0.696 ± 0.112	0.883 ± 0.096	0.917 ± 0.068	0.982 ± 0.063
17	0.959 ± 0.146	0.896 ± 0.084	0.973 ± 0.061	1.003 ± 0.052
18	0.769 ± 0.086	0.883 ± 0.069	1.054 ± 0.059	0.995 ± 0.050
19	0.778 ± 0.080	1.009 ± 0.072	0.848 ± 0.045	0.772 ± 0.038
20	0.818 ± 0.067	0.916 ± 0.063	0.812 ± 0.041	0.884 ± 0.040
21	0.800 ± 0.063	1.322 ± 0.080	1.112 ± 0.053	1.227 ± 0.050
22	0.910 ± 0.069	1.497 ± 0.084	1.378 ± 0.064	1.861 ± 0.074
23	1.378 ± 0.098	1.841 ± 0.111	2.274 ± 0.104	3.110 ± 0.125
24	2.080 ± 0.150	3.051 ± 0.201	3.047 ± 0.165	4.238 ± 0.197
25	3.246 ± 0.297	3.609 ± 0.299	4.711 ± 0.304	5.498 ± 0.285
26	3.716 ± 0.462	6.018 ± 0.807	5.838 ± 0.495	8.162 ± 0.563
27	6.666 ± 1.021	5.647 ± 1.376	8.656 ± 1.046	9.760 ± 0.800

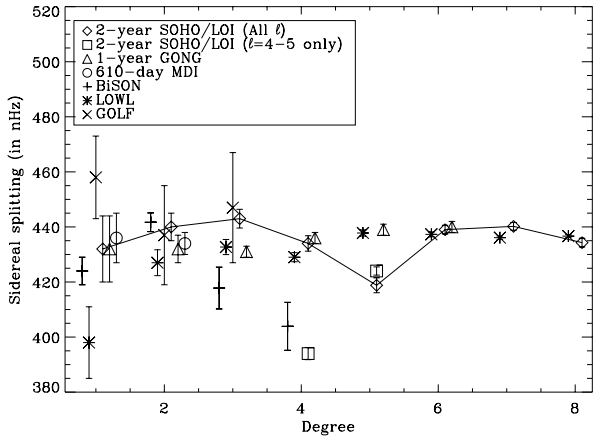

Figure 7: Splitting as a function of l for various instruments. SOHO/LOI data (open diamond): for $l \leq 5$ fitted using Fourier spectra, for $l \geq 6$ fitted using power spectra; (open square) for $l = 4 - 5$ fitted using power spectra. GONG (triangle): from Rabello-Soares and Appourchaux, these proceedings. MDI (open circle) Toutain et al., these proceedings. BiSON (plus) after Chaplin et al.(1996). LOWL (star) after the LOWL home page at HAO. GOLF (cross): Lazrek et al.(1997).

(Appourchaux, 1999, these proceedings). Table 2 gives the sidereal splitting (a_1) for $l \leq 3$.

Figure 7 compare the best low-degree splitting up to date (On the CD-ROM supplement, see file `mmm/appour_2/figure7c.ps`). You can find in the review paper by Appourchaux, these proceedings, a discussion on the possible source of systematic errors for each instrument. From Figure 7, it can be derived that the solar core rotate probably rigidly. This result has been derived by many authors during this conference (Corbard et al.; Eff-Darwich and Korzennik; Rabello-Soares et al., these proceedings).

6. Conclusion

I have analyzed 2 years of LOI data. Systematic errors that are LOI specific are studied in details. I have shown that the solar activity is already affecting the frequencies of the solar p modes. In addition, there is a hint that the linewidth dip may also be affected by the solar activity. The splittings derived from the LOI data makes plausible a solar core rotating at the same rate as the radiative zone. There are still improvements to be made on the p-mode profile model (asymmetry, sloped background noise). Various strategies for reducing systematic errors will also be implemented in the very near future.

Acknowledgements

I would like to express my thanks to the VIRGO team as a whole for putting together this wonderful instrument. I would like to thank Bo Andersen, Claus Fröhlich, Thierry Toutain and Takashi Sekii for endless discussions and/or web chatting. The LOI instrument could not have been put together without the help of Thierry Beaufort, Jos Fleur, Samuel Lévêque, Didier Martin and Udo Telljohann. Thanks to Mohamed Larek for useful comments on the manuscript. Last but not least, many thanks to Koos Planje for the making of the poster(s).

References

Allen, C.W., *Astrophysical Quantities*, 1973, 3rd edition, The Athlone Press, London

Appourchaux, T. & Andersen, B. N., 1990, Sol. Phys., 128, 91

Appourchaux, T., Andersen, B. N., Fröhlich, C., Jimenez, A., Telljohann, U., & Wehrli, C., 1997, Sol. Phys., 170, 27

Appourchaux, T., Chaplin, W. J., Elsworth, Y., Isaak, G. R., McLeod, C. P., Miller, B. A., & New, R. 1997, IAU Symposia, 185, E9

Appourchaux, T., Gizon, L., & Rabello Soares, M. C., 1998a, A&A Sup. Series, 131, in press

Appourchaux, T., Rabello Soares, M. C., & Gizon, L., 1998b, A&A Sup. Series, 131, in press

Appourchaux, T., Toutain, T., Telljohann, U., Jiménez, A., Rabello-Soares, M. C., Andersen, B. N., & Jones, A. R., 1995, A&A, 294, L13

Chaplin, W. J., Elsworth, Y., Isaak, G. R., McLeod, C. P., Miller, B. A., & New, R. 1997, MNRAS, 288, 623

Chaplin, W. J., Elsworth, Y., Howe, R., Isaak, G. R., McLeod, C. P., Miller, B. A., & New, R. 1996, MNRAS, 280, 849

Elsworth, Y., Howe, R., Isaak, G. R., McLeod, C. P., Miller, B. A., New, R., Speake, C. C., & Wheeler, S. J. 1994, ApJ, 434, 801

Fierry-Fraillon, D., Gelly, B., Schmider, F. X., Hill, F., Fossat, E., & Pantel, A. 1998, A&A, 333, 362

Fröhlich, C., Andersen, B. N., Appourchaux, T., Berthomieu, G., Crommelynck, D. A., Domingo, V., Fichot, A., Finsterle, W., Gomez, M. F., Gough, D., Jiménez, A., Leifsen, T., Lombaerts, M., Pap, J. M., Provost, J., Cortés, T. R., Romero, J., Roth, H., Sekii, T., Telljohann, U., Toutain, T., & Wehrli, C., 1997, Sol. Phys., 170, 1

Gizon, L., Appourchaux, T., & Gough, D. O., 1997, IAU Symposia, 185, E6

Gough, D. O. 1977, ApJ, 214, 196

Houdek, G., PhD Thesis, *Pulsation of solar-type stars*, Univeristät Wien, Wien, Austria

Jiménez, A., Gómez, & Zatón, E., 1998, *Sounding solar and stellar interiors*, Janine Provost and Francois-Xavier Schmider eds, p. 39

Lazrek, M., Baudin, F., Bertello, L., Boumier, P., Charra, J., Fierry-Fraillon, D., Fossat, E., Gabriel, A. H., García, R. A., Gelly, B., Gouiffes, C., Grec, G., Pallé, P. L., Hernandez, F. P., Régulo, C., Renaud, C., Robillot, J. -M., Cortés, T. R., Turck-Chièze, S., & Ulrich, R. K. 1997, Sol. Phys., 175, 227

Rabello-Soares, M. C., Roca Cortés, T., Jiménez, A., Appourchaux, T., & Eff-Darwich, A., 1997, ApJ, 480, 840

Ritzwoller, M. H. & Lavely, E. M. 1991, ApJ, 369, 55

Schou, J., 1992, PhD Thesis, *On the analysis of helioseismic data*, Århus universitet, Århus, Denmark

Toutain, T., Appourchaux, T., Baudin, F., Fröhlich, C., Gabriel, A., Scherrer, P., Andersen, B. N., Bogart, R., Bush, R., Finsterle, W., García, R. A., Grec, G., Henney, C. J. , Hoeksema, J. T., Jiménez, A., Kosovichev, A., Cortés, T. R., Turck-Chièze, S., Ulrich, R., & Wehrli, C. 1997, Sol. Phys., 175, 311